

Stable zinc-blende ZnO thin films: formation and physical properties

O. Chichvarina · T. S. Heng · K. C. Phuah ·
W. Xiao · N. Bao · Y. P. Feng · J. Ding

Received: 19 June 2014 / Accepted: 19 August 2014 / Published online: 29 August 2014
© Springer Science+Business Media New York 2014

Abstract The development of technologically important material zinc-blende ZnO has been hindered due to the difficulties inherent in obtaining a stable zinc-blende phase. In this paper, we fabricate the stable zinc-blende ZnO on Pt/Ti/SiO₂/Si substrate through phase transformation from the originally wurtzite to the zinc-blende phase. X-ray diffraction data in combination with high-resolution TEM measurements provide the direct evidence on the formation of the well-defined zinc-blende structure with predominated (202) orientation. According to the experimental results and first principles calculations, the incorporation of titanium dopants into ZnO system favors the formation of the zinc-blende structure. The platinum (Pt) surface stabilizes the ZnO zinc-blende structure at the interface (thin film) due to its low ZnO/Pt interface energy, preventing the decomposition in ZnO wurtzite and Zn₂TiO₄. Additionally, magnetic and optical properties of the ZnO zinc-blende thin films are investigated. Unexpectedly, the film is found to exhibit magnetization of ~ 75 emu/cm³, while its ZnO wurtzite counterpart is non-ferromagnetic.

Introduction

Group II–VI compound semiconductor zinc oxide (ZnO) crystallizes in two main polymorphs with tetrahedral

coordination: hexagonal wurtzite (WZ) and cubic zinc-blende (ZB). The WZ–ZnO with predominated (002) orientation is commonly observed experimentally [1, 2], as it is thermodynamically stable under ambient conditions. In contrast, ZB–ZnO phase is thermodynamically metastable [3]. It showed tendency to be stabilized by heteroepitaxial growth on ZnS/GaAs [4], Al₂O₃ [5], Pt/Ti/SiO₂/Si [6], and other substrates by applying various synthesis techniques, such as metalorganic, sol–gel, molecular-beam epitaxy, etc. However, most of the obtained ZB–ZnO thin films reveal a mixture of phases which comprises both WZ and ZB phases separated by crystallographic defects. In some cases, secondary phases (e.g., ZnS, Zn₂TiO₄, etc.) are present in the ZB–ZnO film, depending on sample preparation technique. It is a material's challenge to obtain single-phase ZB phase due to a tendency to form WZ subdomains within the ZB matrix, though it is of a particular interest due to several technological advantages over WZ. First, the higher crystallographic symmetry of ZB structure facilitates devices fabrication due to its low carrier scattering and higher doping efficiencies [7]. Second, in optoelectronics, with ZnO being the most adaptive candidate for stable room temperature polariton operation [8–14], ZB–ZnO laser microcavities can be easily fabricated along the <110> directions together with the substrate that will lead to higher optical gain [15].

These advantages stimulated many attempts to prepare ZB–ZnO films [4–6, 16]. However, the growth of ZB–ZnO is difficult to achieve, and the underlying mechanism of the ZB formation remains unclear. In this paper, we report a fabrication of ZB–ZnO thin films on Pt/Ti/SiO₂/Si substrates and propose growth mechanism. The films transform from WZ to ZB phase under 900 °C heat treatment, which is attributed to Ti out-diffusion and Pt underlayer effect. A clear Ti-doped ZB structure, (ZnO_xTi_{1-x})O, has

O. Chichvarina · T. S. Heng · K. C. Phuah · W. Xiao ·
N. Bao · J. Ding (✉)
Department of Materials Science and Engineering, National
University of Singapore, 7 Engineering Drive 1,
Singapore 117574, Singapore
e-mail: msedingj@nus.edu.sg

Y. P. Feng
Department of Physics, National University of Singapore, 2
Science Drive 3, Singapore 117542, Singapore

been identified by high-resolution transmission electron microscopy (HRTEM) and X-ray diffraction (XRD) analysis. The first principles calculations support our experimental observations. Furthermore, we observe some unique features of the ZB–ZnO: (1) it has a narrower optical band gap and (2) higher magnetization compared to WZ–ZnO. Our findings pave the way to the realization of ZB–ZnO-based devices.

Experimental methods

ZnO films with thicknesses of ~ 20 and ~ 200 nm were grown on Pt(150 nm)/Ti(50 nm)/SiO₂(300 nm)/Si substrates under oxygen partial pressure of 8×10^{-4} Torr using a pulsed laser deposition (PLD) technique. Relatively low deposition temperature of 200 °C was used to circumvent Ti out-diffusion process during the deposition while maintaining the good crystallinity of the as-prepared films. Subsequently, the samples underwent annealing process in the range of 600–1000 °C for 8 h in open air.

The XRD measurement was performed on Bruker AXS D8 Advance X-ray diffractometer using Cu K α radiation ($\lambda = 1.5418$ Å). The microstructure properties of the films were studied by a high-resolution transmission electron microscope (HRTEM) using a JEOL 100 CX instrument (200 kV). The cross-sectional specimens for TEM study were thinned by mechanical grinding and ion milled to achieve the electron transparency. The photoluminescence (PL) spectra were recorded by means of iHR320 Horiba Jobin–Yvon PL spectroscopy under excitation of HeCd laser (325 nm). The magnetic properties of the samples were measured at room temperature using a vibrating sample magnetometer (VSM) manufactured by the Lakeshore company. The field was applied in-plane of the films. To have a better understanding of the origin of ferromagnetism in the Ti-doped ZnO films, (Zn_{1-x}Ti_x)O, a series of ZnO films with various thicknesses (from 20 to 600 nm) was prepared under identical deposition conditions and annealed at 900 °C.

Further insight into a formation mechanism of ZB, the first principles calculations were performed using Vienna ab initio simulation package (VASP) [17] based on density functional theory (DFT). A supercell of $3 \times 3 \times 2$ was employed in this work for bulk calculation. Cutoff energy was set at 550 eV for the plane-wave basis. In all calculations, ionic relaxations were performed until forces on all ions were <0.02 eV Å⁻¹, while self-consistent accuracy of $<10^{-4}$ eV was achieved for electronic loops. K-point mesh densities were varied with the default VASP-generated Γ -centered Monkhorst–Pack grids [18] as the lowest density used.

Results and discussion

Figure 1a shows typical XRD patterns of ZnO films (both 20 and 200 nm) with a prominent WZ (002) peak. After annealing at 600, 700, and 800 °C ZnO, films retained their ZnO WZ phase with no detection of secondary phases. Beyond 900 °C, a notable phase change has been observed. As revealed by the XRD study, the films were found to possess different phases and compositions (Fig. 1b, c). The XRD spectrum for the thin ZnO films (20 nm) demonstrated (1) a total suppression of the predominated WZ–ZnO (002) peak, (2) disappearance of any WZ–ZnO-related peaks, and (3) the absence of zinc titanate-related secondary phases (Fig. 1c). Instead, the diffraction pattern for these films revealed ZB–ZnO (102) peak at 43.80° and ZB–ZnO (202) peak at 56.61°, which is consistent with previous report [6]. These results clearly indicate the formation of ZB–ZnO after 900 °C open air heat treatment. Furthermore, the lattice constant of ZB–ZnO film appeared to be ~ 4.64 Å, which agrees with its theoretical ZB–ZnO values.

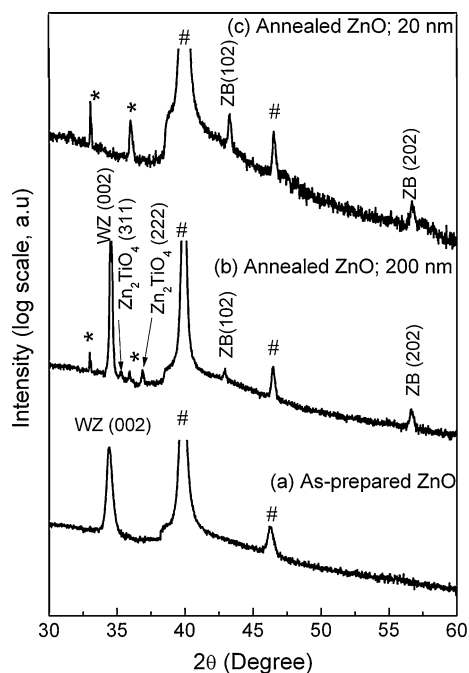


Fig. 1 **a** The XRD study of as-prepared ZnO films (both 20 and 200 nm) showed the well-defined patterns that correspond to WZ–ZnO structure with predominated (002) orientation. **b** In 200 nm film, the mixture phases of WZ–ZnO, ZB–ZnO, and Zn₂TiO₄ were obtained after 900 °C open air annealing. **c** (002) peak vanished after 900 °C open air annealing for the 20 nm film. It was accompanied by the appearance of two peaks identified as zinc-blende ZnO. Pt–Ti phase (marked by asterisk) formed after annealing, indicating the out-diffusion of Ti. The Pt substrate peaks are marked by *ash*

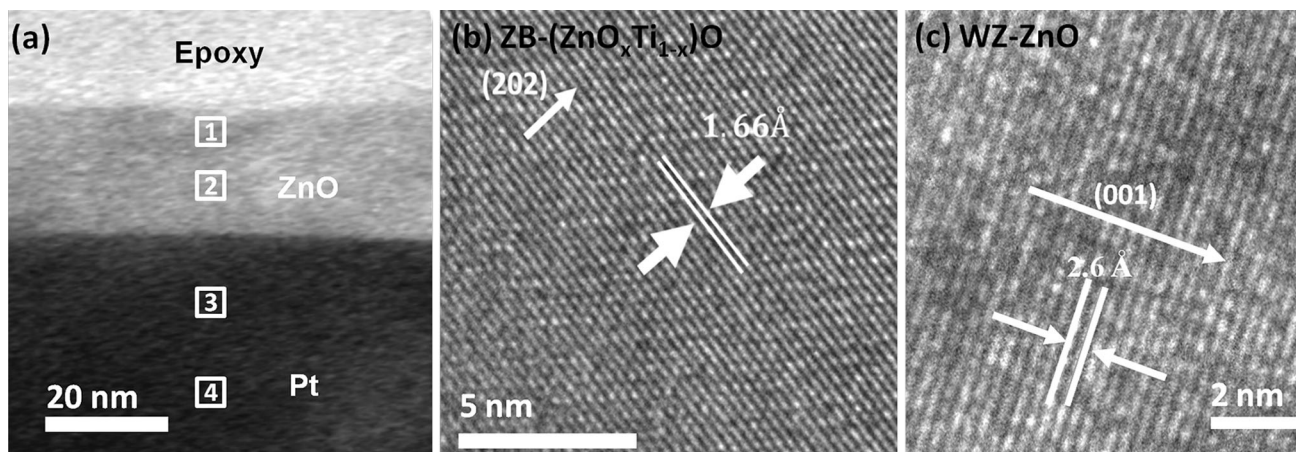


Fig. 2 **a** The cross-sectional transmission electron microscopy (TEM) image of 20 nm ZnO film on substrate after 900 °C open air annealing. The Ti concentrations at position 1, 2, 3, and 4 are ~9, ~10, ~12, and ~13 %, respectively, affirming the out-diffusion of Ti after annealing. **b** The corresponding high-resolution TEM

(HRTEM) image of ZB-(Zn_xTi_{1-x})O film, showing the well-oriented (202) plane with its interplanar distance of ≈ 1.66 Å. **c** The HRTEM image of the as-prepared ZnO film, the well-oriented (002) plane with interplanar distance of ≈ 2.6 Å

In contrast, the thick (200 nm) ZnO films annealed at 900 °C showed the presence of multiple phases such as ZnO WZ (WZ-ZnO), ZnO ZB (ZB-ZnO), and zinc titanate (Zn₂TiO₄), as shown in Fig. 1b. Unlike the thin ZnO films, the thick films had the predominated WZ-ZnO (002) peak. The formation of the Zn₂TiO₄ phase can be explained by the out-diffusion of titanium (Ti) into ZnO under high temperature which agrees with the literature [6]. It should be mentioned that Pt-Ti phases (marked by *asterisk*) were detected after annealing. The same phases were observed in the XRD scans of the Pt/Ti/SiO₂/Si substrates without films annealed under identical conditions.

To gain further insight into phase formation of ZB-ZnO and Ti out-diffusion, the cross-sectional transmission electron microscopy (TEM) imaging was performed. Figures 2a, b show the TEM images of the 20 nm annealed ZnO film. The results demonstrate well-oriented (202) plane with its interplanar distance of 1.66 Å, which corresponds to ZB-ZnO structure. In contrast, the as-prepared ZnO film exhibits the interplanar distance of 2.6 Å that refers to WZ-ZnO structure as shown in Fig. 2c. Moreover, Ti concentration of the samples at various depths was examined by energy-dispersive spectrometer (EDS) attached to the TEM system. It was found that Ti concentration is gradually reduced in bottom-up direction. Figure 2a depicts that the average Ti concentration is ~12.5 % in Pt substrate, whereas it reduces to ~10 % in the ZB-ZnO film (position 2). Approaching the surface of the ZB-ZnO (position 1), the Ti concentration is ~9 %. In the subsequent discussion, we denote our ZB-ZnO films as ZB-(Zn_xTi_{1-x})O due to incorporation of Ti in the film. It is important to emphasize that no Ti element was detected in either as-prepared ZnO film or Pt layer prior to the

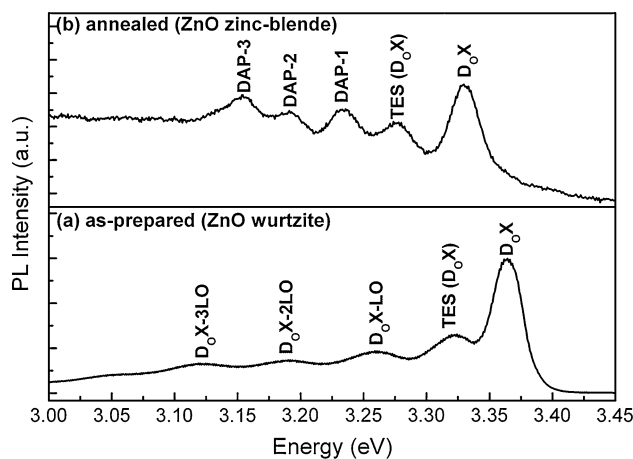


Fig. 3 The low-temperature photoluminescence (PL) of **a** the as-prepared ZnO film (wurtzite phase) and **b** ZB-(Zn_xTi_{1-x})O film after annealing

annealing. This result provides direct evidence that Ti ions have been out-diffused after the annealing which is in agreement with the XRD data.

Apart from the structural properties variation, the WZ-ZnO and ZB-(Zn_xTi_{1-x})O structures have a different band structure and optical property [3, 7]. Thus, low-temperature (5 K) PL was carried out to investigate the optical properties of the WZ-ZnO and ZB-(Zn_xTi_{1-x})O. The as-prepared WZ-ZnO film demonstrates the strongest near-band-edge (NBE) emission peak due to neutral donor bound exciton (D_oX) centered at 3.36 eV as shown in Fig. 3. It is accompanied by two electron satellites (TES) of D_oX at ~3.32 eV. Other three peaks are longitudinal optical (LO) phonon replicas, separated by 0.071–0.073 eV [19] and associated with free and bound excitons. The annealed ZnO

film, however, showed different behaviors. It was found that D_{0X} peak of ZB-(Zn_xTi_{1-x})O film was shifted to lower energy regime by ~ 0.034 eV compared to its WZ-ZnO counterpart, depicting the reduction of optical bandgap after annealing. It is noted that our experimental bandgap narrowing value (~ 0.034 eV) is in the same order as the theoretical value [20]. The bandgap reduction phenomenon is commonly observed in the WZ to ZB transformation process [6] which affirms the formation of ZB phase after annealing.

Based on our structural analysis, Ti dopant certainly plays an essential role in the transformation of WZ into ZB phase. However, recent reports showed that Ti doping in ZnO does not lead to the formation of ZB phase [21, 22]. It was confirmed that ZnO ZB phase can be formed neither by intentional doping of Ti into ZnO [23, 24] nor using Ti or TiO_2 as an underneath layer [25]. These results clearly show that the use of Pt underlayer may play another important role for the formation of ZnO ZB phase.

To understand the underlying growth mechanism of ZB-(Zn_xTi_{1-x})O, the first principles calculations were performed. First, we evaluate the role of Ti and calculate the formation energy of Ti-doped ZnO as a function of Ti concentration, ranging from ~ 3 to ~ 15 %. The formation energy increases with the increase of Ti concentration in ZnO (Fig. 4a). The results suggest that it is possible to form ZB-(Zn_xTi_{1-x})O when the ratio of Ti_{Zn} is < 10 %. The formation is unlikely when Ti concentration is > 10 %. As shown in Fig. 4b, the undoped ZnO has a positive transformation energy (E_T) which indicates that spontaneous transformation from WZ- to ZB-ZnO is impossible. Interestingly, the substitution of Ti (~ 5 – 10 %) into ZnO lowers the E_T to a negative value, making ZB-($Zn_{1-x}Ti_x$)O a more preferable phase than WZ-($Zn_{1-x}Ti_x$)O.

Since the formation energy of ZB-(Zn_xTi_{1-x})O has a positive value (see Fig. 4a), the structure is likely to decompose into energetically favorable mixture phase (e.g., WZ-ZnO, ZB-ZnO, Zn_2TiO_4 , etc.). It agrees with our experimental observations that the thick (200 nm) ZnO film exhibits the mixture phase after annealing. To prevent the growth of the mixture phase, ZB phase should be further stabilized. According to our findings, interface energy between ZnO and Pt substrate is another factor that contributes to ZB-ZnO formation.

Our experimental data clearly demonstrate that Pt underneath layer is essential for the ZB phase formation. The experimental XRD spectra unveiled that (001) alignment is typical for ZnO WZ film, (101) orientation predominates in ZnO ZB, and Pt has predominated peak of (111). Based on these results, we built a model for structural simulation of WZ-ZnO and ZB-ZnO on the Pt (111) surface. Our calculation results unveil that the surface energy of the Pt(111) alone was found to be 2.39 Jm $^{-2}$

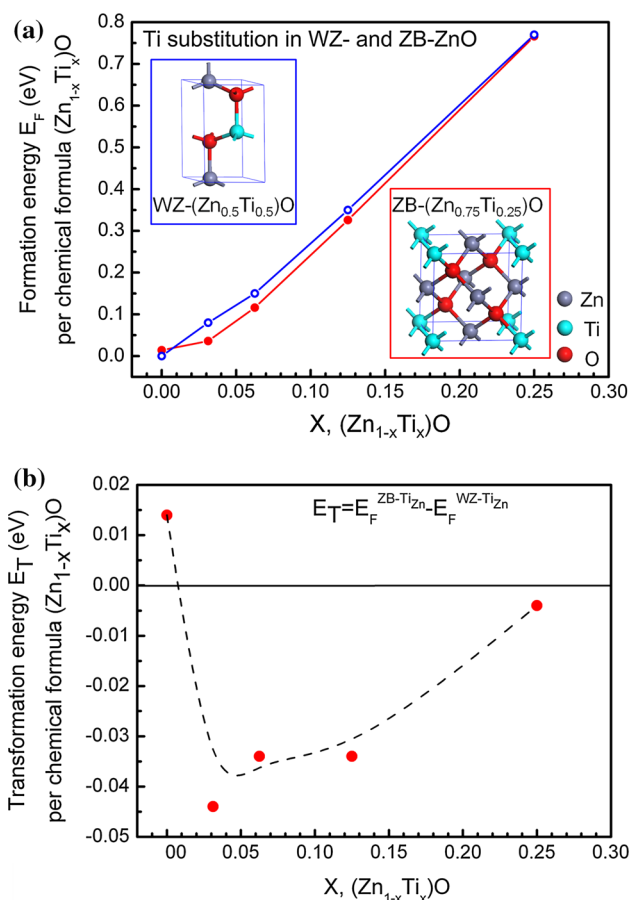


Fig. 4 **a** Formation energy of Ti_{Zn} in WZ- and ZB-ZnO as a function of Ti concentration. Reference energy was set as the energy of most stable phase of WZ-ZnO. Inset: atomic structure of WZ-($Zn_{0.5}Ti_{0.5}$)O and ZB-($Zn_{0.75}Ti_{0.25}$)O cell. **b** Transformation energy E_T from WZ-ZnO to ZB-ZnO structure as a function of Ti concentration

which concurs with the previous reported value [26]. It is noted that the WZ-ZnO film has lower adsorption energy (-7.2 eV) than that of ZB-ZnO (-6.8 eV). Consistently, our experimental results show that the as-deposited layer being of WZ phase regardless its thickness.

In addition, the presence of Zn_2TiO_4 is considered in our subsequent modeling, as it was detected in the thick-annealed ZnO films (Fig. 1). Based on our model, bulk Zn_2TiO_4 is more stable than Ti-substituted ZnO. In the case of thin film, ZnO/Pt(111) has a lower interface energy than Zn_2TiO_4 /Pt(111). Therefore, the Ti-doped ZnO on a Pt (111) substrate exhibits a critical (equilibrium) thickness. Below the critical (equilibrium) thickness, the single-phase ZB-($Zn_{1-x}Ti_x$)O film can be obtained. Above the critical thickness, the mixture phase of WZ-ZnO, ZB-($Zn_{1-x}Ti_x$)O, and Zn_2TiO_4 will be formed. As shown in Fig. 5, the estimated thickness is reversely proportional to the concentration of Ti and demonstrates a phase boundary between single phase of ZB-($Zn_{1-x}Ti_x$)O and mixture

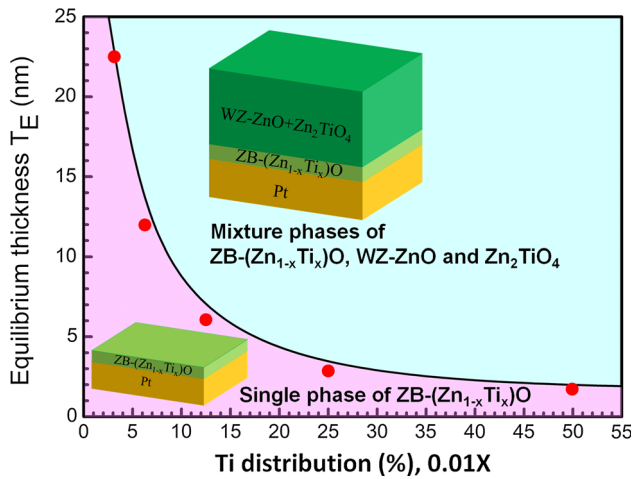


Fig. 5 Equilibrium thickness T_E as a function of Ti concentration (%) demonstrates two distinct regimes. Below the equilibrium thickness (*pink region*), the single-phase ZB-(Zn_{1-x}Ti_x)O is formed. In contrast, the mixture phases of ZB-(Zn_{1-x}Ti_x)O, Zn₂TiO₄, and WZ-ZnO are formed above the equilibrium thickness (*light blue region*) (Color figure online)

phases of ZB-(Zn_{1-x}Ti_x)O, Zn₂TiO₄, and WZ-ZnO. The critical thickness for the formation of ZB-(Zn_{1-x}Ti_x)O on Pt substrate is estimated to be ~ 10 nm for Ti concentration in the range of 5–10 %. It is consistent with experimental results (film thickness ~ 20 nm with Ti concentration of ~ 10 %).

Another striking characteristic of ZnO, ZB phase is its unexpected high magnetization. Figure 6a shows the magnetic hysteresis loops of 20-nm-thick WZ-ZnO and ZB-(Zn_{1-x}Ti_x)O films. Our ZB-(Zn_{1-x}Ti_x)O film exhibits the saturated magnetization of ~ 75 emu/cm³. However, no magnetization was observed for the WZ-ZnO. It is

worthwhile to highlight that there is no ferromagnetism observed in annealed Pt substrate, confirming the observed ferromagnetic signal is contributed by ZB-ZnO.

To have a better understanding of the origin of ferromagnetism in ZB-(Zn_{1-x}Ti_x)O phase, a series of the as-prepared ZnO film with various thicknesses (from 20 to 600 nm) were annealed at 900 °C in open air. The VSM results (Fig. 6b) showed that magnetization value normalized by volume (volume magnetization) is increasing with a decrease of thickness. The saturated volume magnetization is ~ 75 emu/cm³ for 20 nm as compared to ~ 2 emu/cm³ for 650 nm film. The magnetization was also normalized by area (areal magnetization). Surprisingly, no significant change in areal magnetization was observed, regardless its thickness. These results suggest that the observed ferromagnetism is mainly attributed by thin ZB-(Zn_{1-x}Ti_x)O layer (~ 20 nm) at Pt interface. Once the films become thicker, the mixture phase of WZ-ZnO and Zn₂TiO₄ will grow on top of the ZB-(Zn_{1-x}Ti_x)O layer.

Conclusion

In summary, we have prepared a ZB phase of Ti-doped ZnO, ZB-(Zn_{1-x}Ti_x)O thin film by controlling the thickness, Pt/ZnO interface energy, Ti out-diffusion effect, and annealing effect. Below the critical thickness of 20 nm, the WZ-ZnO phase on Pt/Ti/SiO₂/Si substrate transforms into ZB-(Zn_{1-x}Ti_x)O phase after 900 °C annealing. Above its critical thickness, the mixture phase of WZ, ZB, and zinc titanate (Zn₂TiO₄) forms. Based on our calculations, the out-diffusion of Ti into ZnO favors the formation of ZB phase. When the film is thin (<20 nm), the presence of Pt substrate further stabilizes the ZB structure formation.

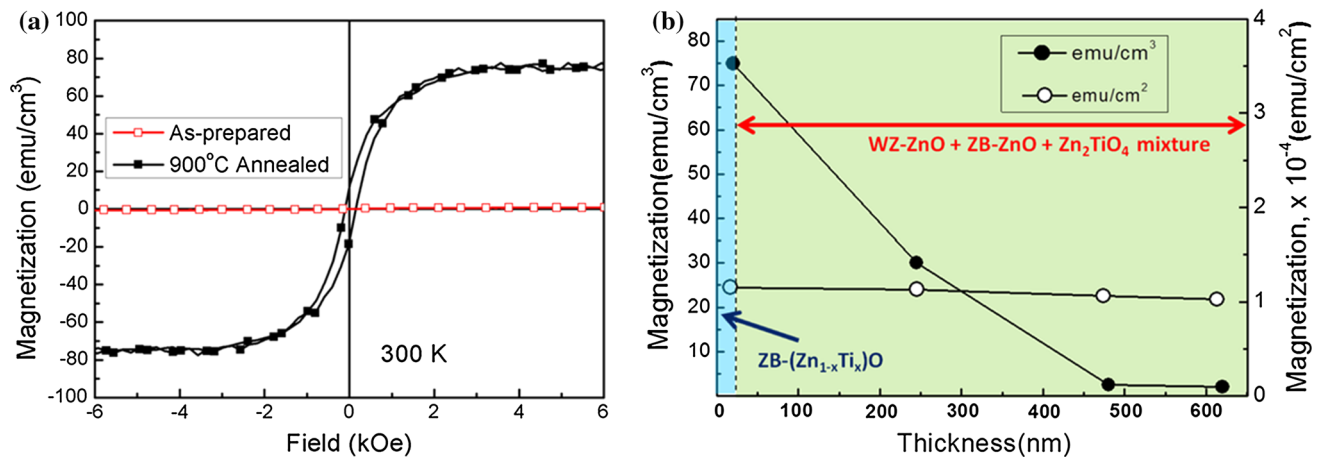


Fig. 6 **a** The room temperature magnetic hysteresis loop of the 20-nm-thick as-prepared WZ-ZnO film and 900 °C annealed ZB-(Zn_{1-x}Ti_x)O film. **b** The thickness-dependent magnetization (emu/cm³ and emu/cm²) of the annealed ZnO films

Acknowledgements This work is supported by A-Star SERC 1321202068, Singapore National Research Foundation under its Competitive Research Funding (NRF-CRP 8-2011-06 and NRF2008NRF-CRP002024), MOE-AcRF-Tier-2 (MOE2010-T2-2-121).

References

- Pearson SJ, Norton DP, Ip K, Heo YW, Steiner T (2003) Recent progress in processing and properties of ZnO. *Superlattices Microstruct* 34(1–2):3–32. doi:[10.1016/s0749-6063\(03\)00093-4](https://doi.org/10.1016/s0749-6063(03)00093-4)
- Herng TS, Kumar A, Ong CS, Feng YP, Lu YH, Zeng KY, Ding J (2012) Investigation of the non-volatile resistance change in noncentrosymmetric compounds. *Sci Rep* 2. doi:<http://www.nature.com/srep/2012/120817/srep00587/abs/srep00587.html#supplementary-information>
- Ozgun U, Alivov YI, Liu C, Teke A, Reshchikov MA, Dogan S, Avrutin V, Cho S-J, Morkoc H (2005) A comprehensive review of ZnO materials and devices. *J Appl Phys* 98(4):041301–041103
- Ashrafi A, Ueta A, Avramescu A, Kumano H, Suemune I, Ok YW, Seong TY (2000) Growth and characterization of hypothetical zinc-blende ZnO films on GaAs(001) substrates with ZnS buffer layers. *Appl Phys Lett* 76(5):550–552. doi:[10.1063/1.125851](https://doi.org/10.1063/1.125851)
- Lee GH, Kawazoe T, Ohtsu M (2002) Difference in optical bandgap between zinc-blende and wurtzite ZnO structure formed on sapphire (0001) substrate. *Solid State Commun* 124(5–6):163–165. doi:[10.1016/s0038-1098\(02\)00537-9](https://doi.org/10.1016/s0038-1098(02)00537-9)
- Kim SK, Jeong SY, Cho CR (2003) Structural reconstruction of hexagonal to cubic ZnO films on Pt/Ti/SiO₂/Si substrate by annealing. *Appl Phys Lett* 82(4):562–564. doi:[10.1063/1.1536253](https://doi.org/10.1063/1.1536253)
- Ashrafi A, Jagadish C (2007) Review of zincblende ZnO: stability of metastable ZnO phases. *J Appl Phys* 102(7):071101
- Lai YY, Lan YP, Lu TC (2013) Strong light-matter interaction in ZnO microcavities. *Light-Sci Appl* 2(6):e76. doi:[10.1038/lsa.2013.32](https://doi.org/10.1038/lsa.2013.32)
- Shimada R, Xie J, Avrutin V, Ozgun U, Morkoc H (2008) Cavity polaritons in ZnO-based hybrid microcavities. *Appl Phys Lett* 92(1):011127. doi:[10.1063/1.2830022](https://doi.org/10.1063/1.2830022)
- Chen JR, Lu TC, Wu YC et al (2009) Large vacuum Rabi splitting in ZnO-based hybrid microcavities observed at room temperature. *Appl Phys Lett* 94:061103. doi:[10.1063/1.3079398](https://doi.org/10.1063/1.3079398)
- Sturm C, Hilmer H, Schmidt-Grund R, Grundmann M (2009) Observation of strong exciton-photon coupling at temperatures up to 410 K. *New J Phys* 11(7):073044. doi:[10.1088/1367-2630/11/7/073044](https://doi.org/10.1088/1367-2630/11/7/073044)
- Chen JR, Lu TC, Wu YC et al (2011) Characteristics of exciton-polaritons in ZnO-based hybrid microcavities. *Opt Express* 19:4101. doi:[10.1364/oe.19.004101](https://doi.org/10.1364/oe.19.004101)
- Orosz L, Reveret F, Bouchoule S et al (2011) Fabrication and optical properties of a fully-hybrid epitaxial ZnO-based microcavity in the strong-coupling regime. *Appl Phys Express* 4(7):072001. doi:[10.1143/apex.4.072001](https://doi.org/10.1143/apex.4.072001)
- Lu TC, Lai YY, Lan YP et al (2012) Room temperature polariton lasing versus photon lasing in a ZnO-based hybrid microcavity. *Opt Express* 20:5530
- Vanmaekelbergh D, van Vugt LK (2011) ZnO nanowire lasers. *Nanoscale* 3(7):2783–2800. doi:[10.1039/c1nr00013f](https://doi.org/10.1039/c1nr00013f)
- Lee GH, Kawazoe T, Ohtsu M (2005) Room temperature near-field photoluminescence of zinc-blend and wurtzite ZnO structures. *Appl Surf Sci* 239(3–4):394–397. doi:[10.1016/j.apsusc.2004.06.004](https://doi.org/10.1016/j.apsusc.2004.06.004)
- Kresse G, Furthmuller J (1996) Efficient iterative schemes for ab initio total-energy calculations using a plane-wave basis set. *Phys Rev B* 54(16):11169–11186. doi:[10.1103/PhysRevB.54.11169](https://doi.org/10.1103/PhysRevB.54.11169)
- Monkhorst HJ, Pack JD (1976) Special points for brillouin-zone integrations. *Phys Rev B* 13(12):5188–5192. doi:[10.1103/PhysRevB.13.5188](https://doi.org/10.1103/PhysRevB.13.5188)
- Teke A, Ozgur U, Dogan S, Gu X, Morkoc H, Nemeth B, Nause J, Everitt HO (2004) Excitonic fine structure and recombination dynamics in single-crystalline ZnO. *Phys Rev B* 70(19):195207. doi:[10.1103/PhysRevB.70.195207](https://doi.org/10.1103/PhysRevB.70.195207)
- Catlow CRA, French SA, Sokol AA, Al-Sunaidi AA, Woodley SM (2008) Zinc oxide: a case study in contemporary computational solid state chemistry. *J Comput Chem* 29(13):2234–2249. doi:[10.1002/jcc.21051](https://doi.org/10.1002/jcc.21051)
- Tseng Y-C, Lin Y-J, Chang H-C, Chen Y-H, Liu C-J, Zou Y-Y (2012) Effects of Ti content on the optical and structural properties of the Ti-doped ZnO nanoparticles. *J Lumin* 132(2):491–494. doi:[10.1016/j.jlumin.2011.08.016](https://doi.org/10.1016/j.jlumin.2011.08.016)
- Lin S-S, Huang J-L, Lii D-F (2005) Effect of substrate temperature on the properties of Ti-doped ZnO films by simultaneous rf and dc magnetron sputtering. *Mater Chem Phys* 90(1):22–30. doi:[10.1016/j.matchemphys.2004.08.040](https://doi.org/10.1016/j.matchemphys.2004.08.040)
- Li HX, Chen Q, Chen XP, Mao QN, Xi JH, Ji ZG (2013) Improvement of resistive switching in ZnO film by Ti doping. *Thin Solid Films* 537:279–284. doi:[10.1016/j.tsf.2013.04.028](https://doi.org/10.1016/j.tsf.2013.04.028)
- Zhong ZY, Zhang T (2013) Microstructure and optoelectronic properties of titanium-doped ZnO thin films prepared by magnetron sputtering. *Mater Lett* 96:237–239. doi:[10.1016/j.matlet.2013.01.025](https://doi.org/10.1016/j.matlet.2013.01.025)
- Lin YC, Hsu CY, Hung SK, Wen DC (2013) Influence of TiO₂ buffer layer and post-annealing on the quality of Ti-doped ZnO thin films. *Ceram Int* 39(5):5795–5803. doi:[10.1016/j.ceramint.2012.12.099](https://doi.org/10.1016/j.ceramint.2012.12.099)
- Needs RJ, Mansfield M (1989) Calculations of the surface stress tensor and surface-energy of the (111) surfaces of iridium, platinum and gold. *J Phys Condens Matter* 1(41):7555–7563. doi:[10.1088/0953-8984/1/41/006](https://doi.org/10.1088/0953-8984/1/41/006)